IEEE Access
Multidisciplinary ⋮ Rapid Review ⋮ Open Access Journal

Received 4 May 2024, accepted 21 May 2024, date of publication 28 May 2024, date of current version 5 June 2024.

Digital Object Identifier 10.1109/ACCESS.2024.3406527

RESEARCH ARTICLE

Bi-Level Deep Unfolding Based Robust Beamforming Design for IRS-Assisted ISAC System

WANXIAN LIU[1], HONGBO XU[1], XIULI HE[1], YUCHEN YE[2], AND AIZHI ZHOU[1]
[1]Department of Electronics and Information Engineering, Central China Normal University, Wuhan 430079, China
[2]School of Electronic Science, National University of Defense Technology, Changsha 410073, China

Corresponding author: Hongbo Xu (xuhb@ccnu.edu.cn)

ABSTRACT In this paper, an intelligent reflecting surface (IRS)-assisted integrated sensing and communication (ISAC) system is considered, where the ISAC base station (BS) serves the communication user equipments (UEs) and tracks sensing targets simultaneously. Unfortunately, it is challenging to obtain the perfect channel state information (CSI) of user equipments (UEs)-related links and target directions in practice. To address the imperfection, we investigate the robust beamforming design under the statistical CSI and bounded target direction uncertainty models. With these considerations, we formulate a Cramér-Rao bound (CRB) of sensing targets minimization problem, subject to the signal-to-interference-plus-noise ratio (SINR) outage probability constraint, the maximum transmit power limits and the unit-modulus constraint of each IRS element. In order to solve this non-convex problem, we formulate the robust beamforming design as a bi-level optimization (BLO) problem and then apply the double-loop deep unfolding (DU) approach to solve this problem. Specifically, we formulate the problem into a primal-dual problem by integrating the SINR outage probability constraint into the objective function which is further approximated by using the worst-case SINR. The projection method and Riemannian manifold optimization method are used to deal with the maximum transmit power constraint and the unit-modulus constraint, respectively. Therefore, the problem can be reformulated as the bi-level optimization (BLO) problem. The lower level (LL) problems aim to find the worst-case CSI and angle of sensing targets. The upper level (UL) problem is the primal-dual problem solved by beamforming design and the Lagrange multipliers optimization with the certain CSI and angle. Then, we apply double-loop DU neural network which unfolds the iterative gradient descent into multi-layer structure, and each layer consists of UL loop and LL loop. In addition, the trainable step sizes and offset parameters are introduced as the network parameters, and the network ultimately outputs optimal optimization variables. Simulation results demonstrate the effectiveness of the proposed robust beamforming design algorithm.

INDEX TERMS Integrated sensing and communication system, intelligent reflecting surface, robust beamforming, bi-level optimization, deep unfolding, worst-case CRB, SINR outage probability.

I. INTRODUCTION

Integrated sensing and communication (ISAC) system which combines the capabilities of communication and sensing within a unified system, holds significant potential in utilizing space-time-frequency resources and has attracted much attention from various areas [1]. Nevertheless, the performance of system remains confined by the limited degrees of freedom, such as the uncontrollable electromagnetic waves propagation. To tackle this issue in ISAC system, the intelligent reflecting surfaces (IRS) has been proposed to enhance the communication and sensing performance [2]. IRS consists of a large number of passive and low-cost reflection elements [3], and the electromagnetic response

The associate editor coordinating the review of this manuscript and approving it for publication was Miguel López-Benítez.

of each reflection element can be tuned by adjusting the phase shift and amplitude [4]. During this process, the IRS consumes no extra power consumption and spectrum resources [5], [6].

Several studies have investigated the performance of IRS-assisted ISAC systems. In [7], the authors aimed to minimize the Cramér-Rao bound (CRB) which provides the lower bound for the variance of any unbiased estimators, subjecting to signal-to-interference-plus-noise ratio (SINR) constraints for the user equipments (UEs) and maximum transmit power. Reference [8] focused on minimizing the transmit power at the ISAC BS subjected to the minimum SINR requirements for both UEs and targets as well as the design of a cross-correlation pattern. Note that the above literature assumes perfect channel state information (CSI) and directions of the sensing targets, which is hard to acquire actually. Therefore, it is necessary to enhance the robustness of beamforming design for the IRS-assisted ISAC system with imperfect CSI and direction of sensing targets [9].

In order to tackle the robust beamforming design, [5] proposed to utilize S-procedure and Conditional value-at-risk (CVaR) based robust transformation approaches, which make the formulated infinite constraint problems become feasible, then introduced an alternate optimization framework that includes successive convex approximation (SCA)-based methods for beamforming design. In [9], the authors utilized the semidefinite relaxation technique and Bernstein-type inequality to transform the problem into a tractable one. Despite showing excellent performance in the robust beamforming design for ISAC system, the primary limit of these iterative algorithms is their high computational complexity which posed a challenge for the real-time implementation [10].

To reduce the complexity, the deep learning (DL) methods have been widely applied for solving beamforming problem. These data driven DL methods learn the mapping relationship between the input and the output through the training process in offline mode and find solutions with trained neural network in the testing stage [11]. The appeal of these approaches is that they can learn any structure of the network through data and make no presumptions on the forward mapping. Therefore, the complexity and real-time requirements are predetermined by the network architecture, which can be satisfied by implementing on a standardized hardware platforms dedicated to DL processing [12]. Regretfully, the data-driven methods are black-box lacking explanation, which results in poor interpretability and weak generalization [13].

Fortunately, the deep unfolding (DU) algorithm is proposed by combining the data-driven approach with the model-driven approach, which naturally incorporates expert knowledge and map the original iterative algorithm into trainable layers [14]. In contrast to black-box DL algorithms, the step sizes of iterative algorithm are transferred into the network parameters, which can be trained using backpropagation [15]. Therefore, the trained neural network can be interpreted as a parameter-optimized method, which effectively addresses the lack of interpretability. In addition, compared with iterative method, the DU algorithm utilized deep neural network to accelerate convergence, while also maintaining performance [16]. Then, the DU approach in [17] unfolded the gradient descent(GD) into multi-layer structure and introduce trainable step sizes and bias parameters, which dramatically decreases the number of trainable parameters.

The DU method is widely applied in the robust beamforming design problem, [18] proposed a DU framework for optimizing the robust beamforming matrix under CSI uncertainty model for multi-user multiple-input multiple-output (MU-MIMO). In [19], the authors leveraged past CSI to enable rapidly, robustly, and interpretability hybrid beamforming design, then unfolded an iterative optimizer for maximizing the minimum data rates under the bounded CSI uncertainty model. The above literature shows excellent performance for robust beamforming design, which inspires us to employ the DU method in our system.

In this paper, we investigate the robust beamforming design for IRS-assisted ISAC system considering the bounded angle uncertainty of sensing targets and statistical CSI uncertainty related to UEs. We formulate a problem aiming to minimize the CRB of sensing targets under SINR outage probability constraint for each UE, the maximum transmit power constraint and the unit-modulus constraint of each IRS reflecting element. However, the problem is non-convex and challenging to solve because of the highly coupled optimization variables and non-linear objective function and constraints. To solve this non-convex problem, we first reformulate the problem into a primal-dual problem by integrating the SINR outage probability constraint into the objective function and approximate SINR outage probability term under statistical CSI uncertainty model by using the worst-case SINR under bounded CSI uncertainty model. Thus, the problem can be viewed as a BLO problem which involves two nested levels (upper level (UL) and lower level (LL)). The UL problem is the primal-dual optimization by optimizing the active beamforming at the ISAC BS and the passive beamforming at the IRS, while LL problems aim to obtain the worst-case uncertainty terms. Then the double-loop DU method is applied to solve this BLO problem by unfolding the iterative double-loop GD into a multi-layer structure. In addition, we obtain the worst-case uncertainty terms in the LL loop and then use them for beamforming design and Lagrangian multipliers optimization in the UL loop.

II. SYSTEM MODEL AND PROBLEM FORMULATION

As depicted in Fig. 1, an IRS-assisted ISAC system is considered where an ISAC BS equipped with N_t transmit antennas serves K single-antenna UEs indexed by $k \in \{1, \cdots, K\}$ and detects Q sensing targets indexed by $q \in \{1, \cdots, Q\}$ simultaneously, while equipped with N_r receive antennas receives echo signals reflected within a scanning

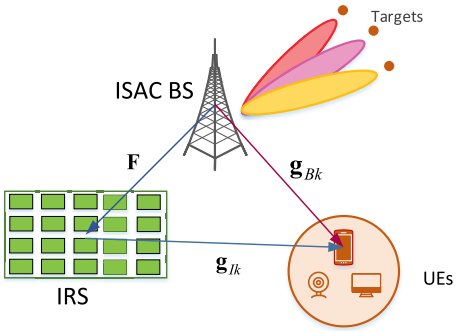

FIGURE 1. System model of IRS-assisted ISAC system.

period T indexed by $t \in \{1, \cdots, T\}$. We make the assumption that $N_t = N_r = N$ in the subsequent analysis [8]. The IRS with M reflecting elements indexed by $m \in \{1, \cdots, M\}$ is deployed to further improve communication and sensing performance.

We consider the transmit signal is jointly precoded by communication and sensing waveform. Let $\mathbf{x}(t)$ denote the transmit signal at the time slot t,

$$\mathbf{x}(t) = \sum_{k=1}^{K} \boldsymbol{\omega}_k c_k(t) + \sum_{j=1}^{N} \boldsymbol{\upsilon}_j s_j(t), \tag{1}$$

where $c_k(t)$ and $s_j(t)$ are the transmit signals for communication UE k and sensing target at time slot t, respectively. $\boldsymbol{\omega}_k \in \mathbb{C}^{N\times 1}$ and $\boldsymbol{\upsilon}_j \in \mathbb{C}^{N\times 1}$ denote the communication and sensing beamforming vectors, respectively. Additionally, we assume $\mathbb{E}\{\mathbf{c}(t)\mathbf{s}^H(t)\} = \mathbf{0}_{K\times N}$, $\mathbb{E}\{\mathbf{c}(t)\mathbf{c}^H(t)\} = \mathbf{I}_K$ and $\mathbb{E}\{\mathbf{s}(t)\mathbf{s}^H(t)\} = \mathbf{I}_N$, where $\mathbf{c}(t) = [c_1(t), \cdots, c_K(t)]^T \in \mathbb{C}^{K\times 1}$ and $\mathbf{s}(t) = [s_1(t), \cdots, s_N(t)]^T \in \mathbb{C}^{N\times 1}$.

In addition, we consider the channel coherence time is greater than T so that the CSI remains stable within a scanning period T. Let $\mathbf{g}_{Bk} \in \mathbb{C}^{N\times 1}$, $\mathbf{g}_{Ik} \in \mathbb{C}^{M\times 1}$ and $\mathbf{F} \in \mathbb{C}^{M\times N}$ denote the complex channel of BS-UE k, IRS-UE k and BS-IRS links in the downlink transmission, respectively. The passive beamforming matrix of the IRS is represented by $\Psi = \text{diag}(\boldsymbol{\vartheta}) \in \mathbb{C}^{M\times M}$ with $\boldsymbol{\vartheta} = [\vartheta_1, \cdots, \vartheta_M]$, where diag$(\cdot)$ denotes the diagonalization operation [20]. The m-th IRS reflection element satisfies the unit-modulus constraint, i.e., $|\vartheta_m| = 1$ [21]. Since the ISAC BS and IRS are fixed in this system, thus, the perfect CSI of BS-IRS link is assumed to be available [22]. However, obtaining perfect CSI of UE-related channel is typically challenging because of the mobility of UEs and unavoidable channel estimation error [5], [9]. In fact, we can only capture the partial distributional information of $\mathbf{g}_{Bk}$ and $\mathbf{g}_{Ik}$. We model the CSI uncertainty terms $\mathbf{g}_{Bk}$ and $\mathbf{g}_{Ik}$ by a statistical uncertainty model [5], i.e.,

$$\mathbf{g}_{Bk} = \hat{\mathbf{g}}_{Bk} + \Delta\mathbf{g}_{Bk}, \quad \mathbf{g}_{Ik} = \hat{\mathbf{g}}_{Ik} + \Delta\mathbf{g}_{Ik}, \tag{2}$$

where $\hat{\mathbf{g}}_{Bk}$ and $\hat{\mathbf{g}}_{Ik}$ are the corresponding estimated channel. $\Delta\mathbf{g}_{Bk} \sim \mathcal{CN}(\mathbf{0}, \Sigma_{Bk})$ and $\Delta\mathbf{g}_{Ik} \sim \mathcal{CN}(\mathbf{0}, \Sigma_{Ik})$ are the uncertainty terms following the independent circularly symmetric complex Gaussian (CSCG) distribution, where $\Sigma_{Bk} \in \mathbb{C}^{N\times N}$ and $\Sigma_{Ik} \in \mathbb{C}^{M\times M}$ are positive semidefinite covariance matrices of $\Delta\mathbf{g}_{Bk}$ and $\Delta\mathbf{g}_{Ik}$, respectively. Then, we define the combined channel from the BS to UE k as

$$\mathbf{h}_k^H = \hat{\mathbf{h}}_k^H + \Delta\mathbf{h}_k^H = (\hat{\mathbf{g}}_{Bk}^H + \hat{\mathbf{g}}_{Ik}^H \Psi\mathbf{F}) + (\Delta\mathbf{g}_{Bk}^H + \Delta\mathbf{g}_{Ik}^H \Psi\mathbf{F}), \tag{3}$$

where the combined CSI uncertainty term $\Delta\mathbf{h}_k = \Sigma_k^{\frac{1}{2}}\mathbf{e}_k \sim \mathcal{CN}(\mathbf{0}, \Sigma_k)$ also follows the CSCG distribution. $\Sigma_k = \Sigma_{Bk} + \Psi\mathbf{F}\mathbf{F}^H\Psi^H\Sigma_{Ik}$ and $\mathbf{e}_k \sim \mathcal{CN}(\mathbf{0}, I)$. In the following, we exploit the combined channel statistical error model for analysis.

Based on the above assumption, the received signal by the UE k at the time slot t is

$$y_k(t) = \mathbf{h}_k^H \boldsymbol{\omega}_k c_k(t) + \sum_{j\neq k}^{K} \mathbf{h}_k^H \boldsymbol{\omega}_j c_j(t) + \sum_{j=1}^{N} \mathbf{h}_k^H \boldsymbol{\upsilon}_j s_j(t) + n_k(t), \tag{4}$$

where $n_k(t) \sim \mathcal{CN}(0, \sigma^2)$ is the addictive white Gaussian noise (AWGN) at the UE k. The second term and the third term in (4) stand for the interference from other UEs and sensing targets, respectively. The SINR of UE k is represented as

$$\gamma_k(\mathbf{W}, \Psi, \{\Delta\mathbf{h}_k\}) = \frac{|\mathbf{h}_k^H \boldsymbol{\omega}_k|^2}{\sum\limits_{j\neq k}^{K} |\mathbf{h}_k^H \boldsymbol{\omega}_j|^2 + \sum\limits_{j=1}^{N} |\mathbf{h}_k^H \boldsymbol{\upsilon}_j|^2 + \sigma^2}, \tag{5}$$

where $\mathbf{W} = [\boldsymbol{\omega}_1, \cdots, \boldsymbol{\omega}_K, \boldsymbol{\upsilon}_1, \ldots, \boldsymbol{\upsilon}_N] \in \mathbb{C}^{N\times(K+N)}$ is the active beamforming matrix at the ISAC BS.

In the occasion of statistical CSI error $\Delta\mathbf{h}_k$, it is difficult to jointly design active and passive beamforming to guarantee a minimum SINR requirement all the time [23]. To accommodate imperfect CSI knowledge, the SINR outage probability is viewed as the communication performance metric [24]. The SINR outage probability refers to the probability that the system will be interrupted when the instantaneous SINR of UE k is lower than a minimum SINR requirement γ_c, represented as

$$\Pr_{\Delta\mathbf{h}_k}\{\gamma_k(\mathbf{W}, \Psi, \{\Delta\mathbf{h}_k\}) \leq \gamma_c\}, \tag{6}$$

where $\Pr_{\Delta\mathbf{h}_k}\{\cdot\}$ calculates the probability of input under statistical CSI error $\Delta\mathbf{h}_k$.

For sensing targets, a fundamental aim is to estimate the directions of the targets, and we assume the direction of arrival (DoA) and the direction of departure (DoD) are the same. However, because of the inevitable estimation errors, the mobility of the sensing targets and so on, the directions of sensing targets can not be acquired accurately in practice, similar to [25] and [26], a bounded uncertainty model is adopted for depicting the angle imperfection at the q-th target, i.e.,

$$\psi_q = \hat{\psi}_q + \Delta\psi_q, \tag{7}$$

where $\hat{\psi}_q$ is the estimated angle of sensing target related to the ISAC BS and the angle uncertainty term satisfies $|\Delta\psi_q| \leq d_q$

where d_q represents the maximum threshold of the bounded angle error.

The received echo signal at the ISAC BS comes from four parts, BS-targets-BS, BS-IRS-BS, BS-IRS-targets-BS and BS-targets-IRS-BS links. However, the echo signals from latter two links are highly attenuated due to three-hop transmissions [8], which has little impact on the system performance. Therefore, we only consider echo signals from the former two links and the received echo signal at the ISAC BS is

$$\mathbf{Y} = \sum_{q=1}^{Q} \zeta_q \mathbf{a}(\psi_q)\mathbf{a}^H(\psi_q)\mathbf{X} + \mathbf{F}^H \Psi \mathbf{F}\mathbf{X} + \mathbf{N}_r, \tag{8}$$

where ζ_q is the complex reflection coefficient of the q-th target. $\mathbf{a}(\psi_q) = [1, e^{-j2\pi\delta\sin(\psi_q)}, \cdots, e^{-j2\pi\delta(N-1)\sin(\psi_q)}]^T \in \mathbb{C}^{N\times 1}$ stands for the steering vector at imperfection direction ψ_q with the normalized antenna spacing δ. We define $\mathbf{A}_q = \mathbf{a}(\psi_q)\mathbf{a}^H(\psi_q)$. $\mathbf{X} = [\mathbf{x}(1), \cdots, \mathbf{x}(T)] \in \mathbb{C}^{N\times T}$ is the transmit signal over the scanning period T. The sample covariance matrix of $\mathbf{X}$ is $\mathbf{R}_\mathbf{X} = \frac{1}{T}\mathbf{X}\mathbf{X}^H \approx \mathbf{W}\mathbf{W}^H$, where the scanning period T is large enough to approximate accurately. $\mathbf{N}_r \sim \mathcal{CN}(0, \sigma_s^2 I_N)$ is the AWGN at the ISAC BS and σ_s^2 denotes the corresponding noise power. Additionally, we make the assumption that the echo signal from the BS-IRS-BS link can be extracted from the received signal via self-interference cancellation (SIC) techniques [27]. However, owing to the demodulation errors or imperfect SIC, there still exists residual interference modeled as $\mathbf{N}_\zeta \sim \mathcal{CN}(0, \sigma_\zeta^2 I_{N_t})$.

We focus on the angle estimation of sensing targets, i.e., estimating the observed parameters $\boldsymbol{\psi} = [\psi_1, \psi_2, \cdots, \psi_Q]^T$. By defining $\tilde{\boldsymbol{\psi}} = [\tilde{\psi}_1, \tilde{\psi}_2, \cdots, \tilde{\psi}_Q]^T$ as the estimated value of $\boldsymbol{\psi}$. We denote the covariance matrix of estimation errors by

$$\text{var}(\boldsymbol{\psi}) = \mathbb{E}[[\tilde{\boldsymbol{\psi}} - \boldsymbol{\psi}][\tilde{\boldsymbol{\psi}} - \boldsymbol{\psi}]^T]. \tag{9}$$

In order to provide the unbiased estimation on the directions of the targets, the CRB is introduced to offer a lower bound of the estimation accuracy [28]. The multiple-parameter CRB states that

$$\text{var}(\boldsymbol{\psi}) \geq C(\boldsymbol{\psi}). \tag{10}$$

The CRB for target q is the diagonal element of the CRB matrix [29], i.e.,

$$C_q = [C(\boldsymbol{\psi})]_{qq} = [F^{-1}]_{qq}, \tag{11}$$

where $\mathbf{F}$ is the Fisher information matrix (FIM). The CRB matrix is the inverse matrix of the FIM [30]. The element in the q-th row and q-th column of $\mathbf{F}$ is [31]

$$[\mathbf{F}]_{qq} = \frac{2T|\zeta_q|^2}{\left(\sigma_s^2 + \sigma_\zeta^2\right)} \text{Tr}(\dot{\mathbf{A}}_q^H \dot{\mathbf{A}}_q \mathbf{R}_\mathbf{X}), \tag{12}$$

where $\dot{\mathbf{A}}_q = \frac{\partial \mathbf{A}_q}{\partial \psi_q} = \dot{\mathbf{a}}(\psi_q)\mathbf{a}^T(\psi_q) + \mathbf{a}(\psi_q)\dot{\mathbf{a}}^T(\psi_q)$ with

$$\dot{\mathbf{a}}(\psi_q) = [0, j2\pi\delta a_2 \cos(\psi_q), \cdots, j2\pi\delta a_{N_t}\cos(\psi_q)]^T, \tag{13}$$

where a_i denotes the i-th entry of $\mathbf{a}(\psi_q)$. The CRB of ψ_q with other targets' directions given is represented as [32]

$$C_q(\mathbf{W}, \{\Delta\psi_q\}) = \frac{(\sigma_s^2 + \sigma_\zeta^2)}{2T|\zeta_q|^2} (\text{Tr}(\dot{\mathbf{A}}_q^H \dot{\mathbf{A}}_q \mathbf{R}_X))^{-1}. \tag{14}$$

In the occasion of bounded error $\Delta\psi_q$, it is difficult to design active beamforming $\mathbf{W}$ to guarantee the CRB of sensing targets. The worst-case CRB of target q is viewed as the sensing performance metric for robust beamforming design, which can be represented as

$$C_q^w(\mathbf{W}, \{\Delta\psi_q^w\}) = \max_{|\Delta\psi_q| \leq d_q} C_q(\mathbf{W}, \{\Delta\psi_q\}). \tag{15}$$

In addition, the sum of worst-case CRBs for all sensing targets in our system is defined as $\text{CRB}_{\text{sum}}^w = \sum_{q=1}^{Q} C_q^w(\mathbf{W}, \{\Delta\psi_q^w\})$.

According to the above analysis, we formulate the sum of worst-case CRBs for all sensing targets minimization problem by jointly optimizing the active beamforming matrix $\mathbf{W}$ and the passive beamforming matrix Ψ,

$$\mathcal{P}^\star: \min_{\mathbf{W},\Psi} \quad \sum_{q=1}^{Q} \max_{|\Delta\psi_q| \leq d_q} C_q(\mathbf{W}, \{\Delta\psi_q\}) \tag{16a}$$

$$\text{s.t. } \text{Pr}_{\Delta\mathbf{h}_k}\{\gamma_k \leq \gamma_c\} \leq \rho_k, \tag{16b}$$

$$\|\mathbf{W}\|_F^2 \leq P_{\max}, \tag{16c}$$

$$|\vartheta_m| = 1, \tag{16d}$$

where $P_{\max}$ is the maximum transmit power of the ISAC BS. $\|\mathbf{W}\|_F$ represents the Frobenius norm of $\mathbf{W}$. Here, the min-max objective function (16a) aims to minimize the sum of the worst-case CRBs of sensing targets under bounded angle uncertainty model. The SINR outage probability constraint (16b) denotes the SINR outage probability of each UE k is not supposed to exceed ρ_k. Constraint (16c) demonstrates the maximum transmit power requirements of the ISAC BS. Constraint (16d) limits each reflection element ϑ_m of the IRS to be unit-modulus.

However, the reasons why the problem is non-convex and difficult to solve lie in 1) the bounded angle uncertainty set in the objective function, 2) the non-convex SINR outage constraint caused by the statistical CSI error model, 3) highly coupled of active beamforming and passive beamforming, 4) the unit-modulus constraints of IRS reflection element. To solve this problem, we will outline our method for addressing the aforementioned challenging presented by problem $\mathcal{P}^\star$ in the next section.

III. JOINT ROBUST ACTIVE AND PASSIVE BEAMFORMING DESIGN ALGORITHM

In this section, we transform the joint robust active and passive beamforming design problem into a BLO problem and apply a double-loop DU based on double-loop GD method for solving the BLO problem.

A. Bi-LEVEL OPTIMIZATION PROBLEM REFORMULATION

Solving the problem $\mathcal{P}^{\star}$ requires jointly optimizing optimization variables over a series of constraints. These can be dealt with partly by integrating the probability constraint into the objection function using the Lagrange multipliers [33]. The Lagrangian function $\mathcal{L}$ can be represented as

$$\begin{aligned}\mathcal{L}(\mathbf{W}, \boldsymbol{\Psi}, \boldsymbol{\lambda}) = &\sum_{q=1}^{Q} C_q(\mathbf{W}, \{\Delta\psi_q\}) \\ &+ \sum_{k=1}^{K} \lambda_k(\Pr_{\Delta\mathbf{h}_k}\{\gamma_k(\mathbf{W}, \Psi, \{\Delta\mathbf{h}_k\}) \\ &\leq \gamma_c\} - \rho_k),\end{aligned} \tag{17}$$

where λ_k is the non-negative Lagrange multiplier which is related to the constraint (16b) and we define $\boldsymbol{\lambda} = [\lambda_1, \cdots, \lambda_K]$. The Lagrangian function can be viewed as an average of objective value and constraint value weighted by their respective multipliers.

Then, we introduce the dual function as the minimum Lagrangian value attained over all optimization variables, given as [34]

$$\mathcal{D}(\boldsymbol{\lambda}) = \min_{\mathbf{W}, \boldsymbol{\Psi}} \mathcal{L}(\mathbf{W}, \boldsymbol{\Psi}, \boldsymbol{\lambda}). \tag{18}$$

It is easy to verify that we have $\mathcal{D}(\boldsymbol{\lambda}) \leq \mathcal{P}^{*}$ for any choice of $\boldsymbol{\lambda} \geq \mathbf{0}$. Therefore, we need to find out $\boldsymbol{\lambda}$ that make $\mathcal{D}(\boldsymbol{\lambda})$ as large as possible.

Then the primal-dual problem can be formulated as

$$2\mathcal{P}2^{\star}: \max_{\boldsymbol{\lambda} \geq \mathbf{0}} \min_{\mathbf{W}, \Psi} \mathcal{L}(\mathbf{W}, \boldsymbol{\Psi}, \boldsymbol{\lambda}) \tag{19a}$$

$$\text{s.t. (16}c\text{), (16}d\text{).} \tag{19b}$$

However, the Lagrangian function $\mathcal{L}(\mathbf{W}, \boldsymbol{\Psi}, \boldsymbol{\lambda})$ consists of the SINR outage probability term based on the CSI statistical uncertainty $\Delta\mathbf{h}_k$, which does not have a close-form expression. To overcome this issue, inspired by the Lemma 1 in [35], the outage probability could be approximated by exploiting the worst-case deterministic function which specifies the ball radius is related to the requirements of the maximum tolerable outage probability.

In our model, the CSI uncertainty follows $\Delta\mathbf{h}_k = \Sigma_k^{1/2}\mathbf{e}_k \sim \mathcal{CN}(\mathbf{0}, \Sigma_k)$. Therefore, the probalbility that $\Delta\mathbf{h}_k$ is located in the region of a $2N$-dimensional ellipsoid with $\mathcal{R} = \{\Delta h_k : \|\mathbf{e}_k\|^2 \leq \mu_k^2\}$ is given by [36]

$$\Pr(\Delta h_k \in \mathcal{R}) = 1 - \rho_k, \tag{20}$$

where $\mu_k = \sqrt{\Phi^{-1}_{\chi^2_{2N}}(1-\rho_k)/2}$ is the ball radius and $\Phi^{-1}_{\chi^2_{2N}}$ is the inverse cumulative distribution function of the (central) Chi-square random variable with $2N$ degrees of freedom [37].

Through the above-mentioned discussion, the following implication holds:

$$\begin{aligned}&\gamma_k(\mathbf{W}, \Psi, \{\Delta\mathbf{h}_k\}) \geq \gamma_c \text{ for all } \|\mathbf{e}_k\| \leq \mu_k \\ &\Rightarrow \Pr_{\Delta\mathbf{h}_k}\{\gamma_k(\mathbf{W}, \Psi, \{\Delta\mathbf{h}_k\}) \geq \gamma_c\} \geq 1 - \rho_k.\end{aligned} \tag{21}$$

The equation (21) suggests that the SINR outage probability under statistical uncertainty model can be approximately in a conservative fashion by the worst-case deterministic SINR under the bounded uncertainty model [35], [38]. Thus, we express the worst-case SINR as

$$\gamma_k^w(\mathbf{W}, \Psi, \{\Delta\mathbf{h}_k^w\}) = \min_{\|\mathbf{e}_k\| \leq d_k} \gamma_k(\mathbf{W}, \Psi, \{\Delta\mathbf{h}_k\}). \tag{22}$$

Therefore, the Lagrangian function can be rewritten as

$$\begin{aligned}&\mathcal{L}_2(\mathbf{W}, \boldsymbol{\Psi}, \boldsymbol{\lambda}) \\ &= \sum_{q=1}^{Q} C_q^w(\mathbf{W}, \{\Delta\psi_q^w\}) \\ &\quad + \sum_{k=1}^{K} \lambda_k(\gamma_k^w(\mathbf{W}, \Psi, \{\Delta\mathbf{h}_k^w\}) - \gamma_c),\end{aligned} \tag{23}$$

where

$$\{\Delta\psi_q^w\} = \operatorname*{argmax}_{\{\Delta\psi_q\}} C_q(\mathbf{W}, \{\Delta\psi_q\}), \tag{24a}$$

$$\{\Delta\mathbf{h}_k^w\} = \operatorname*{argmin}_{\{\Delta\mathbf{h}_k\}} \gamma_k(\mathbf{W}, \Psi, \{\Delta\mathbf{h}_k\}). \tag{24b}$$

In the following, we abbreviate $C_q \triangleq C_q(\mathbf{W}, \{\Delta\psi_q\})$ and $\gamma_k \triangleq \gamma_k(\mathbf{W}, \Psi, \{\Delta\mathbf{h}_k\})$.

Thus, this robust beamforming design problem is transformed into a BLO problem. The LL problems aim to find the worst-case uncertainty terms $\{\Delta\psi_q^w, \Delta\mathbf{h}_k^w\}$, so that we obtain actual angle and combined channel knowledge, given as

$$\psi_q^w = \hat{\psi}_q + \Delta\psi_q^w, \quad \mathbf{h}_k^w = \hat{\mathbf{h}}_k + \Delta\mathbf{h}_k^w. \tag{25}$$

Then, the UL problem can be regarded as a problem to be solved under certain angle and CSI information $\{\psi_q^w, \mathbf{h}_k^w\}$ to obtain optimal active beamforming matrix $\mathbf{W}^{\star}$ and passive beamforming matrix $\boldsymbol{\Psi}^{\star}$.

B. THE Bi-LEVEL OPTIMIZATION BASED ON GRADIENT DESCENT METHOD

In the following, we present the double-loop GD approach for the robust beamforming design. Firstly, this approach consists of double iterative loops, I iterations of UL loop indexed by $i = \{1, \cdots, I\}$ shows the number of GD steps implemented on the UL problem over the optimization variables and Lagrange multipliers. J iterations of LL loop indexed by $j = \{1, \cdots, J\}$ shows the GD steps in terms of the uncertainty terms and worst-case function of the LL problems. Secondly, the GD performed on $\mathcal{L}_2$ of UL loop relies on the $\{\Delta\psi_q^w, \Delta\mathbf{h}_k^w\}$ which is obtained by multiple iterations of LL loop. Finally, the number of iterations of LL loop should be chosen appropriately to balance the accuracy and complexity.

Specifically, we first perform update expressions of LL variables at the j-th iteration of LL loop in the i-th iteration of UL loop, which can be written as

$$\Delta\psi_q^{(i,j+1)} = \Delta\psi_q^{(i,j)} + \tau_1 \nabla_{\Delta\psi_q} C_q, \tag{26a}$$

$$\Delta\mathbf{h}_k^{(i,j+1)} = \Delta\mathbf{h}_k^{(i,j)} - \tau_2 \nabla_{\Delta\mathbf{h}_k} \gamma_k, \tag{26b}$$

where τ_1 and τ_2 are the step sizes. Then, the projection operations $\mathbb{P}(\Delta\psi_q)$ and $\mathbb{P}(\Delta\mathbf{h}_k)$ are adopted to tackle the bounded constraints of uncertainty terms, given as

$$2\mathbb{P}(\Delta\psi_q) = \begin{cases} \Delta\psi_q, & \text{if } |\Delta\psi_q| \le d_q, \\ \dfrac{\Delta\psi_q}{|\Delta\psi_q|} d_q, & \text{otherwise}, \end{cases} \tag{27a}$$

$$\mathbb{P}(\Delta\mathbf{h}_k) = \begin{cases} \Delta\mathbf{h}_k, & \text{if } \|\mathbf{e}_k\| \le \mu_k, \\ \dfrac{\mu_k}{\|\mathbf{e}_k\|}\Delta\mathbf{h}_k, & \text{otherwise} \end{cases} \tag{27b}$$

After the J iterations of LL loop finished, the network outputs the worst-case uncertainty terms $\{\Delta\psi_q^{(i,J)}, \Delta\mathbf{h}_k^{(i,J)}\}$. Then we obtain certain angle and CSI $\{\hat{\psi}_q + \Delta\psi_q^{(i,J)}, \hat{\mathbf{h}}_k + \Delta\mathbf{h}_k^{(i,J)}\}$ for updating the optimization variables and Lagrangian multiplies in the i-th iteration of UL loop.

In the i-th iteration of UL loop, the update of dual-function beamforming matrix $\mathbf{W}$ can be represented as

$$\mathbf{W}^{(i+1)} = \mathbf{W}^{(i)} - \tau_3 \nabla_{\mathbf{W}^{(i)}} \mathcal{L}_2 \left(\mathbf{W}^{(i)}, \boldsymbol{\Psi}^{(i)}, \boldsymbol{\lambda}^{(i)}\right), \tag{28}$$

where τ_3 is the step size. The projection operation $\mathbb{P}(\mathbf{W})$ is utilized to meet maximum transmit power limit (16c), i.e.,

$$\mathbb{P}(\mathbf{W}) = \begin{cases} \mathbf{W}, & \text{if } \|\mathbf{W}\|_F^2 \le P_{\max}, \\ \dfrac{\mathbf{W}}{\|\mathbf{W}\|_F}\sqrt{P_{\max}}, & \text{otherwise}. \end{cases} \tag{29}$$

For updating the passive beamforming matrix of the IRS, we propose to exploit manifold optimization algorithm which can eliminate the unit-modulus constraint (16d) on the product Riemannian manifold. Specifically, denote $\mathcal{M} = \{\boldsymbol{\vartheta} \in \mathbb{C}^{M\times 1} : |\vartheta_m| = 1\}$ as the feasible region of the problem $\mathcal{D}$, and $\tilde{\boldsymbol{\vartheta}}$ is a point on $\mathcal{M}$. The tangent space of $\tilde{\boldsymbol{\vartheta}}$ denoted as $\mathcal{T}_{\tilde{\boldsymbol{\vartheta}}}\mathcal{M}$ is given as

$$\mathcal{T}_{\tilde{\boldsymbol{\vartheta}}}\mathcal{M} = \{\mathbf{z} \in \mathbb{C}^{M\times 1} : \mathrm{Re}\{\mathbf{z} \odot \tilde{\boldsymbol{\vartheta}}^*\} = \mathbf{0}\}, \tag{30}$$

where $\odot$ represents the Hadamard product and $\tilde{\boldsymbol{\vartheta}}^*$ stands for the conjugate of $\tilde{\boldsymbol{\vartheta}}$. Then, we exploit Riemannian gradient which can be acquired by projecting the Euclidean gradient, given as

$$\mathrm{grad}_{\tilde{\boldsymbol{\vartheta}}}\mathcal{L}_2(\mathbf{W}^{(i+1)}, \boldsymbol{\Psi}^{(i)}, \boldsymbol{\lambda}^{(i)}) = \nabla_{\tilde{\boldsymbol{\vartheta}}}\mathcal{L}_2 - \mathrm{Re}\{\nabla_{\tilde{\boldsymbol{\vartheta}}}\mathcal{L}_2 \odot \tilde{\boldsymbol{\vartheta}}^*\} \odot \tilde{\boldsymbol{\vartheta}}, \tag{31}$$

where $\nabla_{\tilde{\boldsymbol{\vartheta}}}\mathcal{L}_2(\mathbf{W}^{(i+1)}, \boldsymbol{\Psi}^{(i)}, \boldsymbol{\lambda}^{(i)})$ is the Euclidean gradient of the $\mathcal{L}_2$ with respect to $\tilde{\boldsymbol{\vartheta}}$. According to Riemannian steepest descent algorithm, $\boldsymbol{\vartheta}$ is iteratively updated by

$$\begin{aligned} \boldsymbol{\vartheta}^{(i+1)} &= \mathcal{R}_{\boldsymbol{\vartheta}^{(i)}}(-\tau_4 \cdot \mathrm{grad}_{\tilde{\boldsymbol{\vartheta}}}\mathcal{L}_2(\mathbf{W}^{(i+1)}, \boldsymbol{\Psi}^{(i)}, \boldsymbol{\lambda}^{(i)}) \\ &= \frac{\boldsymbol{\vartheta}^{(i)} - \tau_4 \cdot \mathrm{grad}_{\tilde{\boldsymbol{\vartheta}}}\mathcal{L}_2(\mathbf{W}^{(i+1)}, \boldsymbol{\Psi}^{(i)}, \boldsymbol{\lambda}^{(i)})}{|\boldsymbol{\vartheta}^{(i)} - \tau_4 \cdot \mathrm{grad}_{\tilde{\boldsymbol{\vartheta}}}\mathcal{L}_2(\mathbf{W}^{(i+1)}, \boldsymbol{\Psi}^{(i)}, \boldsymbol{\lambda}^{(i)})|}, \end{aligned} \tag{32}$$

where $\mathcal{R}_{\boldsymbol{\vartheta}^{(i)}}$ is the retraction operation and τ_4 is the step size. Then $\boldsymbol{\Psi}^{(i+1)} = \mathrm{diag}(\boldsymbol{\vartheta}^{(i+1)})$ to form a diagonalization passive beamforming matrix.

The Lagrange multipliers are updated by maximizing the Lagrangian dual function given as

$$\boldsymbol{\lambda}^{(i+1)} = [\boldsymbol{\lambda}^{(i)} + \tau_5 \nabla_{\boldsymbol{\lambda}}\mathcal{L}_2(\mathbf{W}^{(i+1)}, \boldsymbol{\Psi}^{(i+1)}, \boldsymbol{\lambda}^{(i)})]^+, \tag{33}$$

where τ_5 is the step sizes and $[a]^+ = \max\{0, a\}$ guarantees the non-negative characteristic of the Lagrange multipliers.

Based on the above analysis, the complete procedure is shown in **Algorithm 1**. However, the robust beamforming design based on a double-loop GD approach largely relies on the step sizes which is hard to set appropriately. An unsuitable step sizes could lead to a large number of iterations for convergence [17]. To overcome this difficulty, we propose a double-loop DU method for solving robust beamforming design implementing the trainable step sizes. In addition, the trainable offset parameters are introduced to increase the degrees of freedom [39].

Algorithm 1 The Robust Beamforming Design Based on a Double-Loop GD Approach

Input: Input the estimated channel sample and angle information. Initialize the $\{\mathbf{W}, \boldsymbol{\Psi}, \boldsymbol{\lambda}\}$ and $\{\Delta\psi_q, \Delta\mathbf{h}_k\}$. Set the number of iteration $\boldsymbol{I}$ and $\boldsymbol{J}$ and the step size $\{\tau_1, \tau_2, \tau_3, \tau_4, \tau_5\}$.

1: for $i = 1, \cdots, I$ do
2: for $j = 1, \cdots, J$ do
3: $\Delta\psi_q^{(i,j+1)} = \mathbb{P}(\Delta\psi_q^{(i,j)} + \tau_1 \nabla_{\Delta\psi_q} C_q)$.
4: $\Delta\mathbf{h}_k^{(i,j+1)} = \mathbb{P}(\Delta\mathbf{h}_k^{(i,j)} - \tau_2 \nabla_{\Delta\mathbf{h}_k} \gamma_k)$.
5: Obtain certain angle and CSI $\{\hat{\psi}_q + \Delta\psi_q^{(i,J)}, \hat{\mathbf{h}}_k + \Delta\mathbf{h}_k^{(i,J)}\}$.
6: $\mathbf{W}^{(i+1)} = \mathbb{P}(\mathbf{W}^{(i)} - \tau_3 \nabla_{\mathbf{W}} \mathcal{L}_2(\mathbf{W}^{(i)}, \boldsymbol{\Psi}^{(i)}, \boldsymbol{\lambda}^{(i)})$.
7: $\boldsymbol{\vartheta}^{(i+1)} = \mathcal{R}_{\boldsymbol{\vartheta}^{(i)}}(-\tau_4 \cdot \mathrm{grad}_{\tilde{\boldsymbol{\vartheta}}} \mathcal{L}_2(\mathbf{W}^{(i+1)}, \boldsymbol{\Psi}^{(i)}, \boldsymbol{\lambda}^{(i)})$.
8: $\boldsymbol{\Psi}^{(i+1)} = \mathrm{diag}(\boldsymbol{\vartheta}^{(i+1)})$.
9: $\boldsymbol{\lambda}^{(i+1)} = [\boldsymbol{\lambda}^{(i)} + \tau_5 \nabla_{\boldsymbol{\lambda}} \mathcal{L}_2(\mathbf{W}^{(i+1)}, \boldsymbol{\Psi}^{(i+1)}, \boldsymbol{\lambda}^{(i)})]^+$.

Output: The objective function and optimal optimization variables.

C. THE Bi-LEVEL OPTIMIZATION BASED ON DEEP UNFOLDING METHOD

In this subsection, the robust beamforming design based on a double-loop DU neural network where the trainable step sizes are exploited to accelerate the convergence while maintaining the performance. Specifically, we unfold the hyperparameters of an iterative optimizer with multi-layer and tune them through network training, which transforms the GD into a trainable model [19]. To further enhance the degrees of freedom of the neural network, trainable bias parameters are introduced. The architecture of the proposed algorithm is shown in Fig. 2. In the following, the forward propagation (FP) and back propagation (BP) stage of the proposed algorithm are elaborated carefully.

In the FP stage, we exploit the DU approach as the optimizer with I iterations, we omit the iteration index $i = \{1, \ldots, I\}$ for simplicity in this stage and abbreviate $\mathcal{L}_2(\mathbf{W}, \boldsymbol{\Psi}, \boldsymbol{\lambda}) \triangleq \mathcal{L}_2$. Each iteration consists of U layers of UL loop indexed by $u \in \{1, \ldots, U\}$, and L layers of LL loop indexed by $l \in \{1, \ldots, L\}$ should be implemented firstly at each layer of UL loop. Specifically, the angle and CSI uncertainty term $\{\Delta\psi_q, \Delta\mathbf{h}_k\}$ can be updated via maximizing

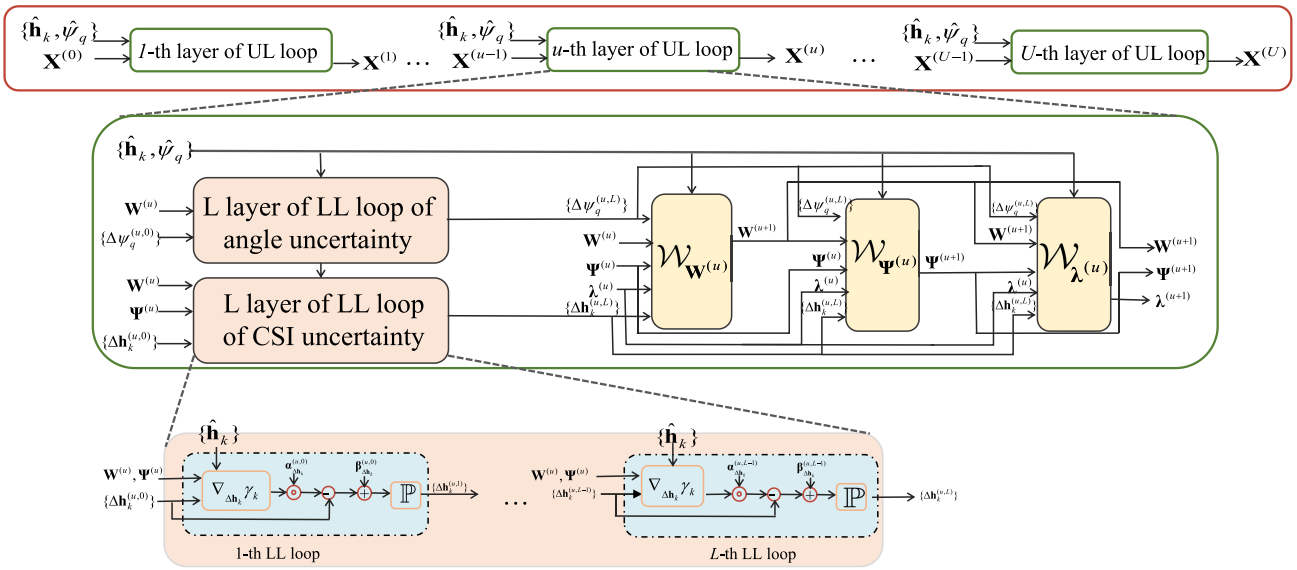

FIGURE 2. The neural network architecture of our proposed algorithm. $\boldsymbol{X} = \{\mathbf{W}, \boldsymbol{\Psi}, \boldsymbol{\lambda}\}$. The update expressions indicated by the $\mathcal{W}_{\mathbf{W}(u)}, \mathcal{W}_{\boldsymbol{\Psi}(u)}, \mathcal{W}_{\boldsymbol{\lambda}(u)}$ corresponding to (35a), (35b) and (33), respectively.

the C_q and minimizing the γ_k, the update expressions at the l-th layer of LL loop in the u-th layer of UL loop are given as

$$\Delta\psi_q^{(u,l+1)} = \mathbb{P}(\Delta\psi_q^{(u,l)} + \alpha_{\Delta\psi_q}^{(u,l)} \cdot \nabla_{\Delta\psi_q} C_q + \beta_{\Delta\psi_q}^{(u,l)}), \quad (34a)$$

$$\Delta\mathbf{h}_k^{(u,l+1)} = \mathbb{P}(\Delta\mathbf{h}_k^{(u,l)} - \boldsymbol{\alpha}_{\Delta\mathbf{h}_k}^{(u,l)} \odot \nabla_{\Delta\mathbf{h}_k} \gamma_k + \boldsymbol{\beta}_{\Delta\mathbf{h}_k}^{(u,l)}), \quad (34b)$$

where $\{\alpha_{\Delta\psi_q}^{(u,l)}, \boldsymbol{\alpha}_{\Delta\mathbf{h}_k}^{(u,l)}\}$ are trainable step sizes to replace the step sizes $\{\tau_1, \tau_2\}$ in (26), and $\{\beta_{\Delta\psi_q}^{(u,l)}, \boldsymbol{\beta}_{\Delta\mathbf{h}_k}^{(u,l)}\}$ are trainable bias parameters. After the L layers of LL loop update finished, we obtain worst-case uncertainty terms $\Delta\psi_q^{(u,L)}$ and $\Delta\mathbf{h}_k^{(u,L)}$ for the u-th layer of UL updates. The update expressions of $\{\mathbf{W}, \boldsymbol{\Psi}, \boldsymbol{\lambda}\}$ at the u-th layer of UL loop are given by

$$\mathbf{W}^{(u+1)} = \mathbb{P}(\mathbf{W}^{(u)} - \boldsymbol{\alpha}_{\mathbf{W}}^{(u)} \odot \nabla_{\mathbf{W}^{(u)}} \mathcal{L}_2 + \boldsymbol{\beta}_{\mathbf{W}}^{(u)}), \quad (35a)$$

$$\boldsymbol{\Psi}^{(u+1)} = \mathrm{diag}(\mathcal{R}_{\boldsymbol{\vartheta}^{(u)}}(-\boldsymbol{\alpha}_{\boldsymbol{\vartheta}}^{(u)} \odot \mathrm{grad}\mathcal{L}_2 + \boldsymbol{\beta}_{\boldsymbol{\vartheta}}^{(u)})), \quad (35b)$$

$$\boldsymbol{\lambda}^{(u+1)} = [\boldsymbol{\lambda}^{(u)} + \boldsymbol{\alpha}_{\boldsymbol{\lambda}}^{(u)} \odot \nabla_{\boldsymbol{\lambda}^{(u)}} \mathcal{L}_2 + \boldsymbol{\beta}_{\boldsymbol{\lambda}}^{(u)}]^+, \quad (35c)$$

where $\{\boldsymbol{\alpha}_{\mathbf{W}}^{(u)}, \boldsymbol{\alpha}_{\Psi}^{(u)}, \boldsymbol{\alpha}_{\boldsymbol{\lambda}}^{(u)}\}$ and $\{\boldsymbol{\beta}_{\mathbf{W}}^{(u)}, \boldsymbol{\beta}_{\Psi}^{(u)}, \boldsymbol{\beta}_{\boldsymbol{\lambda}}^{(u)}\}$ are the trainable step sizes and bias parameters for their corresponding variables.

In the BP stage, the network continuously adjusts the trainable network parameters by minimizing the loss function $\mathcal{L}_2$. We obtain $\mathbf{X}^U = \{\mathbf{W}^{(U)}, \boldsymbol{\Psi}^{(U)}, \boldsymbol{\lambda}^{(U)}\}$ at last layer of UL loop for computing the loss function $\mathcal{L}_2$. Then, the Adam optimizer is implemented to update the trainable parameters, thus the update of the trainable step sizes and bias parameters of ψ_q at the i-th iteration are given by

$$\alpha_{\Delta\psi_q}^{(i+1,u,l)} = \alpha_{\Delta\psi_q}^{(i,u,l)} + \zeta_1^i \cdot \mathrm{Adam}(\nabla_{\alpha_{\Delta\psi_q}} \mathcal{L}_2), \quad (36a)$$

$$\beta_{\Delta\psi_q}^{(i+1,u,l)} = \beta_{\Delta\psi_q}^{(i,u,l)} + \zeta_2^i \cdot \mathrm{Adam}(\nabla_{\beta_{\Delta\psi_q}} \mathcal{L}_2), \quad (36b)$$

Algorithm 2 The Robust Beamforming Based on a Double-Loop DU Neural Network

Input: Input the estimated channel sample and angle information. Initialize the $\{\mathbf{W}, \boldsymbol{\Psi}, \boldsymbol{\lambda}\}$ and $\{\Delta\psi_q, \Delta\mathbf{h}_k\}$. Set the number of layer U, L, the Iteration number I, batch size B and the learning rates ζ_1 and ζ_2 of the network parameters.

repeat
  for $b = 1, \cdots, B$ do
    for $u = 1, \cdots, U$ do
      for $l = 1, \cdots, L$ do
        Update $\Delta\psi_q^{(u,l)}$ and $\Delta\mathbf{h}_k^{(u,l)}$ according to (34).
      Obtain certain angle and CSI $\{\hat{\psi}_q + \Delta\psi_q^{(u,L)}, \hat{\mathbf{h}}_k + \Delta\mathbf{h}_k^{(u,L)}\}$.
      Update $\{\mathbf{W}^{(u+1)}, \boldsymbol{\Psi}^{(u+1)}, \boldsymbol{\lambda}^{(u+1)}\}$ according to (35).
  Calculate average gradient in a batch.
  Update the network parameters via (36).
  Update the iteration number : $i = i+1$.
until the algorithm meets convergence.

Output: The objective function and the optimal optimization variables.

where ζ_1^i and ζ_2^i denote the learning rates in the i-th iteration. Other trainable step sizes and bias parameters are updated as the same way.

The proposed beamforming design algorithm based on a double-loop DU neural network is summarized in **Algorithm 2**.

D. COMPLEXITY ANALYSIS

From the perspective of computation complexity, the proposed double-loop DU method in the testing stage

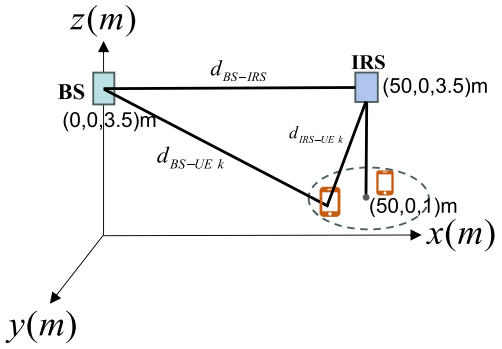

FIGURE 3. Simulation setup for the IRS-assisted ISAC system.

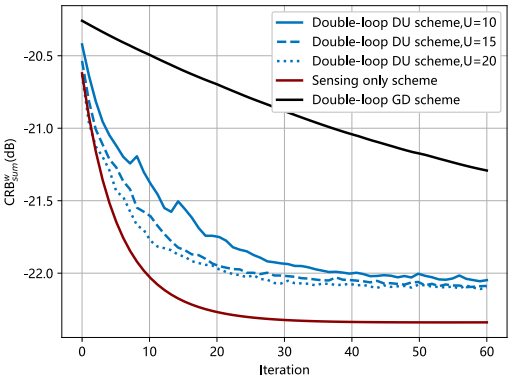

FIGURE 4. The $\mathrm{CRB}_{\mathrm{sum}}^{w}$ versus the number of iteration.

is $\mathcal{O}\left(US(KN+N^2+M+(1+KN)L)\right)$, where S is the size of testing stage. The double-loop GD method is $\mathcal{O}\left(IS(KN+N^2+M+(1+KN)J)\right)$. In fact, for a comparable level of performance, we find $U \ll I$ and $J = L$, which means that the double-loop DU network can effectively reduce the computational complexity compared to its iterative double-loop GD counterpart.

IV. NUMERICAL RESULTS

In this section, numerical results are provided to verify the effectiveness of our proposed robust beamforming design based on a double-loop DU neural network for the IRS-assisted ISAC system.

A three-dimensional coordinate setup is considered, which is shown in Fig.3. The ISAC BS equipped with $N = 8$ antennas is located at (0, 0, 3.5) m, the IRS with $M = 40$ reflecting elements is deployed at (50, 0, 3.5) m, and $K = 4$ UEs are uniformly and randomly distributed in a circle centered at (50, 0, 1) m with a radius 2 m. For large-scale fading, the distance-dependent path loss is modeled by $P = 10^{-3}(d)^{-\alpha}$, where d is the distance between two devices and the path loss exponents $\alpha_{\text{BS-IRS}}$, $\alpha_{\text{BS-UE}}$, and $\alpha_{\text{IRS-UE}}$ are 3.6, 2.2 and 2.2, respectively. For small-scale fading, $\hat{\mathbf{g}}_{Bk}$ follows Rayleigh fading, while $\hat{\mathbf{g}}_{Ik}$ and $\mathbf{F}$ follow Rician fading, where the Rician factor $\kappa = 5$dB [8]. We model the covariance matrices of channel uncertain terms as $\Sigma_{Bk} = \delta^2\|\hat{\mathbf{g}}_{Bk}\|^2\mathbf{I}_N$ and $\Sigma_{Ik} = \delta^2\|\hat{\mathbf{g}}_{Ik}\|^2\mathbf{I}_M$ where $\delta^2 = 0.075$ is used to indicate the relative amount of channel uncertainty. In addition, we consider $L = 3$ targets at the estimated directions of $[-45°, 0°, 45°]$ with respect to ISAC BS and maximum angle uncertainty $d_q = 4°$. The sensing SNR is defined as $\gamma_s = |\zeta_q|^2 TP_{\max}/(\sigma_s^2 + \sigma_\zeta^2)$. Unless otherwise specified, we set $\sigma^2 = -80$dBm, $P_{\max} = 30$dBm, $\gamma_c = 0$ dB, $\gamma_s = -5$dB and $\rho_k = 0.05$.

We compare our proposed scheme with several benchmark schemes, 1) Sensing only scheme [40]: The BS only serves the sensing targets. 2) Without IRS scheme [8]: The ISAC BS directly communicates with the UEs without the help of IRS. 3) Random IRS scheme [41]: The phase shifts of the IRS are randomly initialized without optimizing the passive beamforming matrix. 4) Double-loop GD scheme: The active and passive beamforming are optimized based on the double-loop GD algorithm, as developed in Section III-B. 5)Non-robust scheme [42]: the beamforming optimization is based on the estimated CSI and angle of sensing targets, and the SINR of UEs and CRBs of sensing targets are calculated according to the actual CSI and angle.

For our proposed scheme, the network is trained with a training dataset of 1000 channels over 20 epochs. We set the batch size as $B = 20$, iteration number is $I = 60$, the number of outer layers as $U = 15$ and inner layer as $L = 3$. In addition, robust beamforming design are evaluated over 100 unseen test channels. The Adam optimizer is used for the model training, the decaying learning rate and initial learning rate of 0.99 and 0.0001, respectively. The trainable step sizes are based on empirical observations which are also used as the fixed step sizes for the double-loop GD algorithm. The trainable step sizes are initialized as $\boldsymbol{\alpha}_{\mathbf{W}}^{(0,u)} = 0.1$, $\boldsymbol{\alpha}_{\boldsymbol{\Psi}}^{(0,u)} = 1$ and $\boldsymbol{\alpha}_{\boldsymbol{\lambda}}^{(0,u)} = 0.001$ for $u = 1, \cdots, U$.

Figure 4 depicts the sum of worst-case CRBs for all sensing targets $\mathrm{CRB}_{\mathrm{sum}}^{w}$ versus the number of iterations for different schemes. It is observed that the $\mathrm{CRB}_{\mathrm{sum}}^{w}$ decreases with the number of iteration and converges for our proposed double-loop scheme and sensing only scheme. Sensing only scheme gets best performance since they emphasize sensing only. In addition, we can see that the double-loop DU beamforming algorithm significantly improves the convergence speed of the double-loop GD algorithm. As the number of the layers of UL-loop U increased, the performance of double-loop DU algorithm will be improved. However, increasing U leads to an increase in computational complexity. In order to balance the complexity and performance, we choose $U = 15$ in our paper.

Figure 5 shows the sum of worst-case CRBs for all sensing targets $\mathrm{CRB}_{\mathrm{sum}}^{w}$ versus the communication SINR requirement γ_c. Due to the increasing γ_c of the UEs, the objective function becomes higher for all three schemes. This is because more resources are allocated to guarantee the minimum SINR requirement, resulting in sacrificing the sensing performance. In addition, the proposed scheme outperforms the without IRS and random IRS schemes,

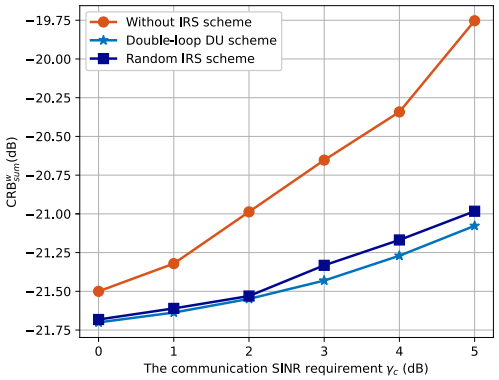

FIGURE 5. The $\mathrm{CRB}^{w}_{\mathrm{sum}}$ versus the SINR requirement γ_c of UEs.

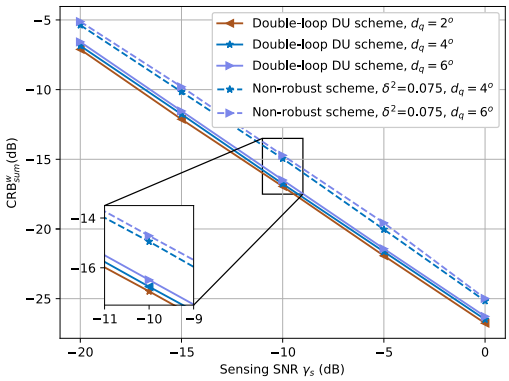

FIGURE 6. The $\mathrm{CRB}^{w}_{\mathrm{sum}}$ versus the sensing SNR.

because the IRS can provide an additional reflection link for higher combined channel gain, which can be further enhanced by optimizing passive beamforming matrix.

Figure 6 depicts the sum of worst-case CRBs for all sensing targets $\mathrm{CRB}^{w}_{\mathrm{sum}}$ versus different sensing SNR γ_s. We observe that the $\mathrm{CRB}^{w}_{\mathrm{sum}}$ is tight in the high SNR regime and with the angle uncertainty bound becomes looser, the performance of $\mathrm{CRB}^{w}_{\mathrm{sum}}$ will deteriorate. In fact, at high sensing SNR values, the useful signals are not too much corrupted by noise, thus, the sensing signals are very informative about the DOA estimates. In addition, compared to the non-robust ISAC beamforming design, the $\mathrm{CRB}^{w}_{\mathrm{sum}}$ obtain a lower value. Thus, compared with the non-robust scheme, the proposed robust beamforming design exhibits robustness against uncertainty.

V. CONCLUSION

In this paper, we investigated the robust beamforming design under the imperfection directions of sensing targets and CSI. The problem was formulated as the worst-case CRBs minimization problem subject to the SINR outage probability constraint, maximum transmit power limit and unit-modulus constraint of IRS reflection element. Then, we proposed the robust beamforming design based on a double-loop DU neural network to solve the reformulated BLO problem. The numerical results verify that the effectiveness of proposed scheme with regard to the convergence behavior, the trade-off between communication and sensing performance and robustness against uncertainty.

REFERENCES

[1] J. A. Zhang, F. Liu, C. Masouros, R. W. Heath, Z. Feng, L. Zheng, and A. Petropulu, "An overview of signal processing techniques for joint communication and radar sensing," *IEEE J. Sel. Topics Signal Process.*, vol. 15, no. 6, pp. 1295–1315, Nov. 2021.

[2] X. Song, J. Xu, F. Liu, T. X. Han, and Y. C. Eldar, "Intelligent reflecting surface enabled sensing: Cramér–Rao bound optimization," *IEEE Trans. Signal Process.*, vol. 71, pp. 2011–2026, 2023.

[3] Z. Lin, H. Niu, K. An, Y. Hu, D. Li, J. Wang, and N. Al-Dhahir, "Pain without gain: Destructive beamforming from a malicious RIS perspective in IoT networks," *IEEE Internet Things J.*, vol. 11, no. 5, pp. 7619–7629, Mar. 2024.

[4] J. Xiao, J. Wang, Z. Wang, W. Xie, and Y. Liu, "Multi-scale attention based channel estimation for RIS-aided massive MIMO systems," *IEEE Trans. Wireless Commun.*, early access, p. 1, Nov. 8, 2023, doi: 10.1109/TWC.2023.3329387.

[5] M. Luan, B. Wang, Z. Chang, T. Hämäläinen, and F. Hu, "Robust beamforming design for RIS-aided integrated sensing and communication system," *IEEE Trans. Intell. Transp. Syst.*, vol. 24, no. 6, pp. 6227–6243, Jun. 2023, doi: 10.1109/TITS.2023.3248145.

[6] D. Li, "Ergodic capacity of intelligent reflecting surface-assisted communication systems with phase errors," *IEEE Commun. Lett.*, vol. 24, no. 8, pp. 1646–1650, Aug. 2020.

[7] Z. Xu, F. Liu, and A. Petropulu, "Cramér–Rao bound and antenna selection optimization for dual radar-communication design," in *Proc. IEEE Int. Conf. Acoust., Speech Signal Process. (ICASSP)*, May 2022, pp. 5168–5172.

[8] M. Hua, Q. Wu, C. He, S. Ma, and W. Chen, "Joint active and passive beamforming design for IRS-aided radar-communication," *IEEE Trans. Wireless Commun.*, vol. 22, no. 4, pp. 2278–2294, Apr. 2023.

[9] P. Liu, Z. Fei, X. Wang, B. Li, Y. Huang, and Z. Zhang, "Outage constrained robust secure beamforming in integrated sensing and communication systems," *IEEE Wireless Commun. Lett.*, vol. 11, no. 11, pp. 2260–2264, Nov. 2022.

[10] W. Xia, G. Zheng, Y. Zhu, J. Zhang, J. Wang, and A. P. Petropulu, "A deep learning framework for optimization of MISO downlink beamforming," *IEEE Trans. Commun.*, vol. 68, no. 3, pp. 1866–1880, Mar. 2020.

[11] H. Hojatian, J. Nadal, J.-F. Frigon, and F. Leduc-Primeau, "Unsupervised deep learning for massive MIMO hybrid beamforming," *IEEE Trans. Wireless Commun.*, vol. 20, no. 11, pp. 7086–7099, Nov. 2021.

[12] J. Yang and Y. Cai, "A novel efficient deep unfolding algorithm based on WMMSE for downlink beamforming," in *Proc. 3rd Asia–Pacific Conf. Commun. Technol. Comput. Sci. (ACCTCS)*, Feb. 2023, pp. 330–334.

[13] Z. Yang, J.-Y. Xia, J. Luo, S. Zhang, and D. Gunduz, "A learning-aided flexible gradient descent approach to MISO beamforming," *IEEE Wireless Commun. Lett.*, vol. 11, no. 9, pp. 1895–1899, Sep. 2022.

[14] J. R. Hershey, J. L. Roux, S. Watanabe, S. Wisdom, Z. Chen, and Y. Isik, "Novel deep architectures in speech processing," in *New Era for Robust Speech Recognition: Exploiting Deep Learning*. Cham, Switzerland: Springer, 2017, pp. 135–164, doi: 10.1007/978-3-319-64680-0_6.

[15] V. Monga, Y. Li, and Y. C. Eldar, "Algorithm unrolling: Interpretable, efficient deep learning for signal and image processing," *IEEE Signal Process. Mag.*, vol. 38, no. 2, pp. 18–44, Mar. 2021.

[16] L. Pellaco, M. Bengtsson, and J. Jaldén, "Matrix-inverse-free deep unfolding of the weighted MMSE beamforming algorithm," *IEEE Open J. Commun. Soc.*, vol. 3, pp. 65–81, 2022.

[17] S. Shi, Y. Cai, Q. Hu, B. Champagne, and L. Hanzo, "Deep-unfolding neural-network aided hybrid beamforming based on symbol-error probability minimization," *IEEE Trans. Veh. Technol.*, vol. 72, no. 1, pp. 529–545, Jan. 2023.

[18] J. Xu, C. Kang, J. Xue, and Y. Zhang, "A fast deep unfolding learning framework for robust MU-MIMO downlink precoding," *IEEE Trans. Cognit. Commun. Netw.*, vol. 9, no. 2, pp. 359–372, Apr. 2023.

[19] O. Lavi and N. Shlezinger, "Learn to rapidly and robustly optimize hybrid precoding," *IEEE Trans. Commun.*, vol. 71, no. 10, pp. 5814–5830, Oct. 2023, doi: 10.1109/TCOMM.2023.3292472.

[20] D. Li, "How many reflecting elements are needed for energy- and spectral-efficient intelligent reflecting surface-assisted communication," *IEEE Trans. Commun.*, vol. 70, no. 2, pp. 1320–1331, Feb. 2022.

[21] J. Wang, J. Xiao, Y. Zou, W. Xie, and Y. Liu, "Wideband beamforming for RIS assisted near-field communications," 2024, *arXiv:2401.11141*.

[22] C. Huang, R. Mo, and C. Yuen, "Reconfigurable intelligent surface assisted multiuser MISO systems exploiting deep reinforcement learning," *IEEE J. Sel. Areas Commun.*, vol. 38, no. 8, pp. 1839–1850, Aug. 2020.
[23] A. Haqiqatnejad, F. Kayhan, and B. Ottersten, "Robust SINR-constrained symbol-level multiuser precoding with imperfect channel knowledge," *IEEE Trans. Signal Process.*, vol. 68, pp. 1837–1852, 2020.
[24] Y. Chen, M. Wen, L. Wang, W. Liu, and L. Hanzo, "SINR-outage minimization of robust beamforming for the non-orthogonal wireless downlink," *IEEE Trans. Commun.*, vol. 68, no. 11, pp. 7247–7257, Nov. 2020.
[25] D. Xu, X. Yu, D. W. K. Ng, A. Schmeink, and R. Schober, "Robust and secure resource allocation for ISAC systems: A novel optimization framework for variable-length snapshots," *IEEE Trans. Commun.*, vol. 70, no. 12, pp. 8196–8214, Dec. 2022.
[26] N. Su, F. Liu, and C. Masouros, "Secure radar-communication systems with malicious targets: Integrating radar, communications and jamming functionalities," *IEEE Trans. Wireless Commun.*, vol. 20, no. 1, pp. 83–95, Jan. 2021.
[27] X. Wang, Z. Fei, and Q. Wu, "Integrated sensing and communication for RIS assisted backscatter systems," *IEEE Internet Things J.*, vol. 10, no. 15, pp. 13716–13726, Aug. 2023, doi: 10.1109/JIOT.2023.3262867.
[28] Z. Cheng, S. Shi, Z. He, and B. Liao, "Transmit sequence design for dual-function radar-communication system with one-bit DACs," *IEEE Trans. Wireless Commun.*, vol. 20, no. 9, pp. 5846–5860, Sep. 2021.
[29] Z. Zhao, L. Zhang, R. Jiang, X.-P. Zhang, X. Tang, and Y. Dong, "Joint beamforming scheme for ISAC systems via robust Cramér–Rao bound optimization," *IEEE Wireless Commun. Lett.*, vol. 13, no. 3, pp. 889–893, Mar. 2024.
[30] R. Liu, M. Li, Q. Liu, and A. L. Swindlehurst, "SNR/CRB-constrained joint beamforming and reflection designs for RIS-ISAC systems," *IEEE Trans. Wireless Commun.*, early access, p. 1, Dec. 18, 2023, doi: 10.1109/TWC.2023.3341429.
[31] Z. Ren, Y. Peng, X. Song, Y. Fang, L. Qiu, L. Liu, D. W. K. Ng, and J. Xu, "Fundamental CRB-rate tradeoff in multi-antenna ISAC systems with information multicasting and multi-target sensing," *IEEE Trans. Wireless Commun.*, vol. 23, no. 4, pp. 3870–3885, Apr. 2024.
[32] X. Wang, Z. Fei, J. Huang, and H. Yu, "Joint waveform and discrete phase shift design for RIS-assisted integrated sensing and communication system under Cramer–Rao bound constraint," *IEEE Trans. Veh. Technol.*, vol. 71, no. 1, pp. 1004–1009, Jan. 2022.
[33] M. Eisen, C. Zhang, L. F. O. Chamon, D. D. Lee, and A. Ribeiro, "Learning optimal resource allocations in wireless systems," *IEEE Trans. Signal Process.*, vol. 67, no. 10, pp. 2775–2790, May 2019.
[34] H. Huang, M. Liu, G. Gui, H. Gacanin, H. Sari, and F. Adachi, "Unsupervised learning-inspired power control methods for energy-efficient wireless networks over fading channels," *IEEE Trans. Wireless Commun.*, vol. 21, no. 11, pp. 9892–9905, Nov. 2022.
[35] K.-Y. Wang, A. M. So, T.-H. Chang, W.-K. Ma, and C.-Y. Chi, "Outage constrained robust transmit optimization for multiuser MISO downlinks: Tractable approximations by conic optimization," *IEEE Trans. Signal Process.*, vol. 62, no. 21, pp. 5690–5705, Nov. 2014.
[36] J. Wang, S. Han, S. Xu, and J. Li, "SNR-outage-based robust artificial noise-aided beamforming for correlated MISO wiretap channels under Gaussian channel uncertainties," *IEEE Syst. J.*, vol. 17, no. 1, pp. 1569–1580, Mar. 2023.
[37] A. Pascual-Iserte, D. Palomar, A. Perez-Neira, and M. Lagunas, "A robust maximin approach for MIMO communications with imperfect channel state information based on convex optimization," *IEEE Trans. Signal Process.*, vol. 54, no. 1, pp. 346–360, Dec. 2006.
[38] X. Chen, S. Xu, S. Han, J. Wang, and W. Meng, "SINR-OP based robust AN-aided beamforming for correlated MISO eavesdropping channels," in *Proc. IEEE Int. Conf. Commun.*, Jun. 2021, pp. 1–5.
[39] X. He, H. Xu, J. Wang, W. Xie, X. Li, and A. Nallanathan, "Joint active and passive beamforming in RIS-assisted covert symbiotic radio based on deep unfolding," *IEEE Trans. Veh. Technol.*, early access, pp. 1–6, Apr. 25, 2024, doi: 10.1109/TVT.2024.3393724.
[40] Z. Ren, L. Qiu, J. Xu, and D. W. K. Ng, "Robust transmit beamforming for secure integrated sensing and communication," *IEEE Trans. Commun.*, vol. 71, no. 9, pp. 5549–5564, Jun. 2023.
[41] Z. Lin, H. Niu, K. An, Y. Wang, G. Zheng, S. Chatzinotas, and Y. Hu, "Refracting RIS-aided hybrid satellite-terrestrial relay networks: Joint beamforming design and optimization," *IEEE Trans. Aerosp. Electron. Syst.*, vol. 58, no. 4, pp. 3717–3724, Aug. 2022.
[42] D. An, J. Hu, Y. Zuo, K. Zhong, X. Xiao, H. Li, and L. Li, "Robust transceiver design for ISAC systems via product complex circle-sphere manifold method," *IEEE Trans. Instrum. Meas.*, vol. 73, pp. 1–14, 2024.

WANXIAN LIU received the B.E. degree in electrical engineering and automation from Hubei University of Technology, China, in 2021. She is currently pursuing the M.S. degree in information and communication engineering with Central China Normal University. Her current research interests include resource allocation, beamforming design, and beyond 5G communication.

HONGBO XU received the M.S. degree in radio electronics from Central China Normal University, Wuhan, China, in 1997, and the Ph.D. degree from the Institute for Pattern Recognition Artificial Intelligence, Huazhong University of Science and Technology, Wuhan, in 2005. Since September 2005, he has been an Associate Professor with Central China Normal University. His research interests include signal processing, mobile edge computation, and wireless communication.

XIULI HE received the B.S. degree in applied physics from Zhongyuan University of Technology, China, in 2021. She is currently pursuing the M.S. degree in radio physics with Central China Normal University. Her current research interests include deep learning and covert communication.

YUCHEN YE received the B.E. degree in electronic information science and technology from Central China Normal University, China, in 2018. She is currently pursuing the M.S. degree in electronics science and technology with the National University of Defense Technology. Her current research interests include resource allocation and performance evaluation with integrated sensing and communication systems.

AIZHI ZHOU received the Ph.D. degree from the School of Physics, Peking University, Beijing, China, in 2003. She is currently an Associate Professor with the School of Physics, Central China Normal University, Wuhan, China. Her research interests include data processing and big data engineering.